Actuators

Deutsche Ausgabe: DOI: 10.1002/ange.201507108
Internationale Ausgabe: DOI: 10.1002/anie.201507108

# A Mechanically Actuating Carbon-Nanotube Fiber in Response to Water and Moisture

*Sisi He, Peining Chen, Longbin Qiu, Bingjie Wang, Xuemei Sun, Yifan Xu, and Huisheng Peng**

***Abstract:*** *A new family of hierarchically helical carbon-nanotube fibers with many nano- and micro-scale channels has been synthesized. They demonstrate remarkable mechanical actuations in response to water and moisture. The water or moisture is first rapidly transported through the trunk micron-scale channels and then efficiently infiltrates into the interconnected capillary nanoscale channels, similar to the blood flow in our body. Therefore, rapid and large contraction and rotation of the fiber occurs with a high reversibility. These mechanically actuating fibers are promising for various applications, and smart windows and louvers have been investigated as two demonstrations.*

Water is of great importance as an environmental stimulus to trigger movements and transport that are essential reactions in living systems, particularly plants.[1] Leaves push upwards because of shrinkage upon evaporation of water inside, pine cones open upon water absorption and awns propel into the soil in response to moisture.[2] The principle of these movements relies on the swelling and shrinking of the micro-fluidic water-conducting cellulose fibrils in the plant upon water absorption and evaporation.[3] In these biological materials, hierarchically assembled structures are critical to realize such functionalities.[4] For instance, upon making contact with water, *Towel Gourd* tendril's elongation occurs owing to a hierarchy of chirality caused by the arrangement of molecules, microfibrils, cellulose fibrils, cells, tendril filaments to the macroscopic tendril helix in the tendril.[5] A humidity change causes seed pods to open owing to the existence of hierarchical composite materials made of stiff cellulose fibrils embedded in a softer non-cellulosic matrix.[6]

Inspired by the nature, a variety of materials including polymers, shape-memory alloys, metal oxides, and ceramics have been designed with hierarchical architectures for actuating devices.[7] These hierarchical materials are capable of converting the change of external stimuli, such as electricity, temperature, magnetic field, and solvent, into mechanical work. However, they have been typically made into thin films that generally bend along a specific direction, or bulk materials that simply swell/shrink in all dimensions in response to the external stimuli. It is difficult to realize some desired complex while tunable actuations. In addition, they share some disadvantages, such as low stress, slow response, and low stability, which limit their practical applications in sensing.[8]

Carbon nanotubes (CNTs) are one of the most explored building blocks for mechanical actuators owing to their unique structure and combination of mechanical, electronic, and thermal properties.[9] Importantly, aligned CNT fibers, that have been demonstrated to extend the excellent physical properties of individual CNTs to a macroscopic scale, have been extensively investigated for actuators.[10] Among them, the CNT fiber actuators based on thermal, electrochemical, and electromagnetic mechanisms exhibit superb actuation performances.[11] However, to our knowledge, fiber actuators that are composed of aligned CNTs and that mechanically respond to water/moisture have not been realized yet owing to the hydrophobic nature of CNTs, although such actuators are critical for a variety of applications.

Herein, we have designed hierarchically helical channels with hydrophilic surfaces in aligned CNT fibers to offer a rapid and large contraction and rotation with a high reversibility in response to water and moisture. These novel fiber actuators exhibit promising applications in many fields, and smart windows and louvers that react in response to water and moisture are investigated as two demonstrations.

To prepare a hydrophilic and hierarchically helical CNT fiber, a hydrophilic primary fiber (HPF) fabricated from a pristine primary CNT fiber was first obtained (Figure 1 a). The pristine primary CNT fiber was twisted from an aligned CNT sheet that had been dry-drawn from a spinnable array.[12] The CNTs had a multi-walled structure with an average diameter of around 10 nm (Figure S1 in the Supporting Information). The chirality and helical angle were tuned by varying the twisting direction and speed, respectively (Figure S2 and S3). A large number of interconnected channels at nanoscale, typically from tens to hundreds of nanometers in diameter, were formed among the aligned CNTs due to their helically aligned organizations. The resulting CNT fiber was modified to be hydrophilic after an oxygen plasma treatment (Figure 1 a): The surface of the pristine primary fiber was hydrophobic with a water contact angle of 138.6°; it became hydrophilic after an oxygen plasma treatment with a power of 100 W for 15 min (insets in Figure 1 c,e). Importantly, in comparison to the traditionally modified methods for CNTs such as chemical methods,[13] no obvious damage was observed for the aligned structure in CNTs after the plasma treatment, and the nano-channels among the aligned CNTs had also been well maintained (Figure 1 b,d and Figure S4). Additionally, the preparation of the fiber could be easily

[*] S. He, P. Chen, L. Qiu, Dr. B. Wang, Dr. X. Sun, Y. Xu, Prof. Dr. H. Peng
State Key Laboratory of Molecular Engineering of Polymers, Collaborative Innovation Center of Polymers and Polymer Composite Materials, Department of Macromolecular Science and Laboratory of Advanced Materials, Fudan University
Shanghai 200438 (China)
E-mail: penghs@fudan.edu.cn

Supporting information for this article is available on the WWW under http://dx.doi.org/10.1002/anie.201507108.

  

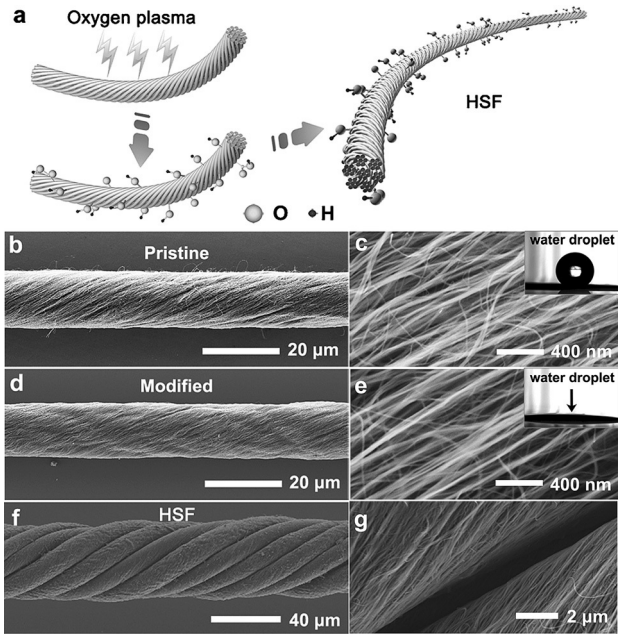


***Figure 1.*** Preparation of HSFs with hierarchically helical channels. a) Schematic illustration to the preparation. b), c) SEM images of a pristine primary CNT fiber at low and high magnifications, respectively. d), e) SEM images of an HPF after plasma modification at low and high magnifications, respectively. The insets in (c) and (e) indicate the non-wetted and wetted contacts between a water droplet and CNTs before and after an oxygen plasma treatment, respectively. f), g) SEM images of a ten-ply HSF after plasma modification at low and high magnifications, respectively.

scaled up for practical applications. A roll of a continuous HPF with a length of about 3 m was readily obtained by this method (Figure S5). Multiple HPFs could be further assembled into a hydrophilic secondary fiber (HSF) through a similar twisting process (Figure 1 f). In the resulting HSF, a lot of micron-channels formed between the HPFs (Figure 1 f,g).

The oxygen content of CNTs could be tuned by varying the power and time of oxygen plasma treatment (Table S1). For instance, an oxygen weight percentage of 10.9 % was produced at 300 W for 15 min as verified by energy-dispersive X-ray spectra. It was increased to 11.8 % by using an increased power of 400 W for 15 min or 17.5 % with the prolonging time to 45 min at 300 W. The higher oxygen content was attributed to the increasing number of carbon–oxygen groups with the increasing treatment power and time (Figure S6 and Table S2). Importantly, no obvious changes had been detected for the nano-channels among the aligned CNTs even at high oxygen contents (Figure S7). Note that the pristine primary CNT fiber also showed an oxygen weight percentage of 3.2 % probably owing to the defects pre-exiting at the CNTs.

In comparison with pristine fibers, the tensile strengths of the HPFs were unexpectedly enhanced. It was increased to 353.8 MPa with an oxygen weight percentage of 5.6 %, 1.4 times of the pristine fiber (250.6 MPa). However, the further increase in the oxygen content decreased their mechanical properties, for example, 248.2 MPa at an oxygen content of 10.9 %, almost the same to the pristine fiber. This phenomenon may be explained by the stronger interaction among aligned CNTs after the introduction of a moderate number oxygen-containing functional groups, but more damage may be produced in the CNTs exposed to the longer oxygen plasma treatment, as detected by the Raman spectra (Figure S8).

The HPF generated an excellent contractive actuation in response to water. Upon coming in contact with a water droplet, a contractive stress of approximately 10.8 MPa was rapidly generated by the HPF within 400 ms with a peak stress rate of 25.3 MPa $s^{-1}$ (Figure S9). It rapidly returned to the original state after removal of the water droplet. The contractive stresses could be tuned by varying their helical angles and oxygen contents in the HPF. For the HPF with an oxygen weight percentage of 10.9 %, the contractive stresses were first increased and then decreased with the increasing helical angle, and a peak value of 10.8 MPa occurred at a helical angle of 20° (Figure S10). The contractive stress was also largely affected by the oxygen content. The contractive stresses were gradually increased with the increasing oxygen content, reaching 22.4 MPa at an oxygen content of 17.5 %. It is more than 200 times that of the typical skeletal muscle and even twice of the pristine CNT fiber driven by electricity.[11a,14] This is probably caused by the increasing oxygen content (Figure S11) which provided higher capacities for water absorption. However, the fiber with a higher oxygen content of 17.5 % showed a relatively lower tensile strength of 141.0 MPa. Therefore, the HPF with an oxygen weight percentage of 10.9 % and helical angle of 20° are discussed below unless specified otherwise, for simplicity. Note that the hydrophobic bare CNT fiber could also generate a contractive stress upon contacting with an organic solvent, such as ethanol (Figure S12).

The contractive and rotary actuations of the helically assembled fibers are attributed to the volume expansion of the helices.[11b,c] The volume expansion can be regarded as a result of water infiltration through capillary forces based on the following two facts. One, the channels formed in the fiber provide considerable capacity for solvent infiltration. Two, it has been demonstrated that the contact angles of water against modified CNTs are far below 90° (Figure 1 e). Thus, the fibers can be rapidly wetted by water according to Young's Equation. The actuations of graphene and graphene oxide (GO) fibers triggered by moisture have been also explored previously,[15,16] which is attributed to the volume expansion of graphene oxide sheets after infiltration of water. A larger rotation was produced by freeing one end of the GO fiber. However, the GO fiber exhibited a relatively slower responsiveness owing to its lack of internal channels, and its mechanical strength was degraded after water infiltration. In contrast, the HPF exhibited a high mechanical stability to water. Both structure and tensile strength of HPF are well maintained after soaking in water for 240 h (Figure S13 and S14).

The multi-layered HPF can be assembled into the HSF to further enhance the contractive and rotary actuation outputs (Figure S15). The contractive forces were linearly increased with the increasing number of HPFs, and the stress outputs

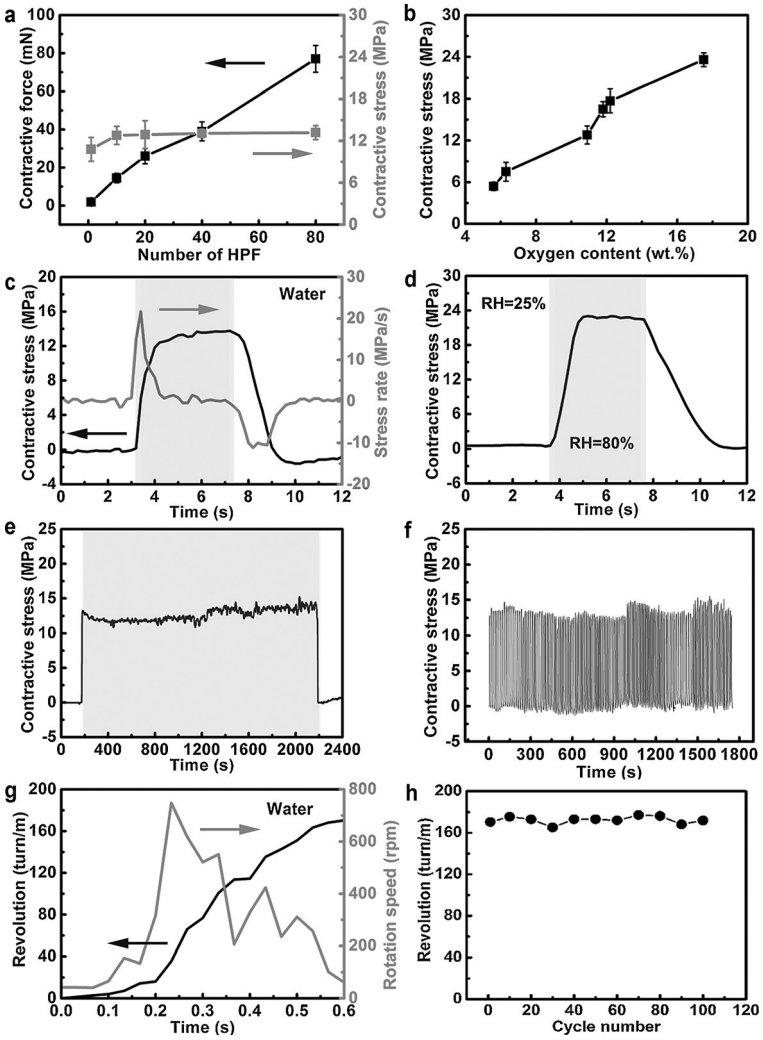


***Figure 2.*** Water-induced contractive and rotatory actuations generated by the HSF. a) Dependence of contractive force (black line) and stress (gray line) generated by the HSF on the number of building HPFs. b) Dependence of contractive stress by the HSF on the oxygen content. c) A typical contractive stress curve (black line) and the corresponding stress rate curve (gray line) of an HSF upon absorption and removal of a water droplet. d) A typical contractive stress curve (black line) and the corresponding stress rate curve (gray line) of an HSF upon the change of humidity. e) Dependence of contractive stress generated by an HSF under the absorption of water for over 2000 s. f) Contractive stresses in response to the water for 100 cycles. g) Dependence of number of revolutions (black line) and rotary speed (gray line) on the time when an HSF came in contact with a droplet of water. h) Dependence of revolution on the cycle number.

reached a plateau of approximately 13.5 MPa at the number of ten HPFs (Figure 2a). The stress could be further improved by increasing the oxygen content of the HPFs (Figure 2b). The HSF from ten-ply HPFs with an oxygen content of 10.9% were explored. A contractive stress of about 13.6 MPa was rapidly generated by an HSF upon coming in contact with a water droplet. The corresponding peak stress rate was 21.7 MPa $s^{-1}$ (Figure 2c). As expected, the HSF also responded to moisture (Figure 2d). A contractive stress of about 22.8 MPa was rapidly generated once the fiber (with a length of 5 mm) was exposed to a moist air with a relative humidity of $\geq 80\%$. The contractive stress was much higher than that caused by contact with a water droplet, probably because a longer part of the fiber was exposed to the moisture compared with a water droplet for the same HSF. When the HSF was immersed into water droplet for over 2000 s, the generated contractive stress had been well maintained at about 14.0 MPa without decay, indicating a high actuation durability in response to water (Figure 2e). In addition, no noticeable decreases in the contractive stress were observed after 100 cycles (Figure 2f). The HSF also exhibited a high actuation reversibility in response to moisture.

Besides the contractive actuation, a rotary actuation was also generated by the HSF upon exposure to water. (Figure 2g). The metal paddle with a weight 23200 times that of the HSF was fixed at the middle of the HSF fiber. The actuations were recorded by a high-speed camera. The dependence of revolution and rotation speed on the time was obtained through a frame-by-frame analysis. Typically, when the upper half of the hydrophilic CNT fiber came in contact with a droplet of water, a marked clockwise rotation was generated. When the lower half of the fiber came in contact with a water droplet, the paddle rotated in an anticlockwise direction (Movie S1). A rotatory actuation of 170.3 turns per meter was generated, which is over 40 times of the electrically driven CNT fiber and two to three orders of magnitude of torsional actuators based on shape-memory alloys and conducting polymers.[11a,17] The moment of inertia of the metal paddle was calculated as $1.2\times10^{-9}$ kg $m^{-2}$. The maximal acceleration generated by the paddle was 80.4 rad·$s^{-2}$ (9220.4°·$s^{-2}$), so the maximal torsional torque ($\tau$) was calculated as 0.4 N·m $kg^{-1}$according to $\tau = I\alpha$, approximately 5 times that of a twisted graphene oxide fiber in response to humidity[16] and close to the commercial electric motor (the Aerotech model 1410-01motor).[18] The rotary actuation was highly reversible upon the absorption and evaporation of water, and the number of revolution generated by the fiber was varied in less than 5% in 100 cycles of actuations (Figure 2i). The highly rotary reversibility is attributed to the fact that the two ends of the actuating fiber are both clamped.[11b,c] The rotation direction could be tuned by varying the chirality of the fibers. Specifically, a clockwise rotation was generated by a left-handed HSF twisted from multi-ply left-handed HPFs, while an anticlockwise rotation was generated by a right-handed HSF twisted from multi-ply right-handed HPFs.

The contractive force could also be enhanced by increasing the diameter of HPF that twisted from multi-layer CNT sheets (Figure S16). However, the HSF and HPF with the similar diameter were different in the response. More specifically, the HSF twisted from ten HPFs generated a higher contraction output and faster responsiveness than

  

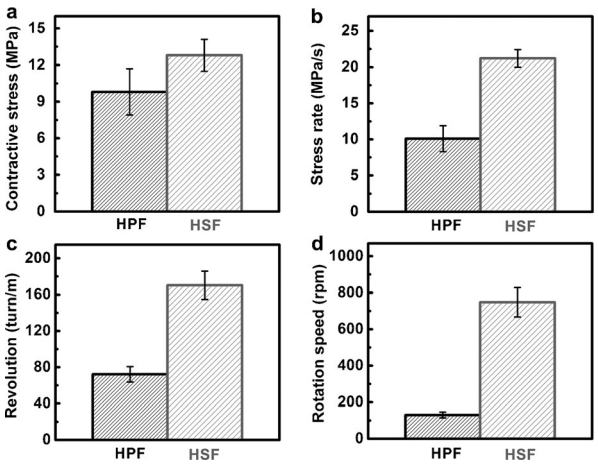


***Figure 3.*** Comparison between the HSF and HPF with the same diameter. a)–d) Actuation performances between an HSF (light column) twisted from ten HPFs and an HPF (dark column) twisted from ten-layer CNT sheets.

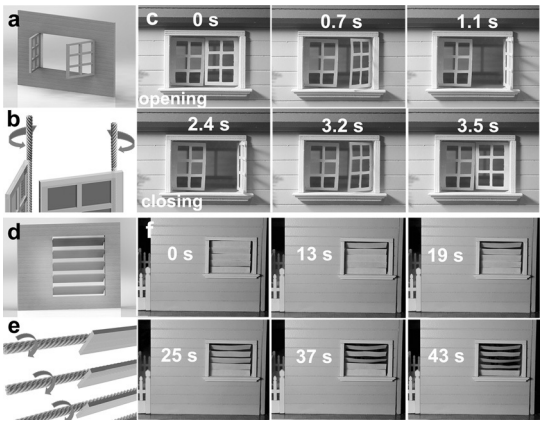


***Figure 4.*** Smart window in response to water and louver in response to moisture. a), b) Schematic illustration to the smart window. c) Photographs in tracing the opening and closing process of the window in response to water. d), e) Schematic illustration to the smart louver. f) Photographs in tracing the opening process of the louver in response to moisture.

the counterpart HPF twisted from ten layers of stacked CNT sheets (Figure 3 a,b). The stress rate generated by the former was twice of the later. The HSF twisted from ten HPFs also generated a faster revolution and rotation speed than the counterpart HPF twisted from ten layers of stacked CNT sheets (Figure 3 c,d), and the revolution and the rotation speed generated by the HSF twisted from HPFs was more than twice and four times those of the HPF twisted from stacked CNT sheets, respectively. The different actuations may be explained by the difference in the channels formed inside. For the HSF twisted from HPFs, there are hierarchically helical channels at nano- and micron-scales, while only nanoscale helical channels were available in the large HPF twisted from stacked multi-layered CNT sheets (Figure S17). The hierarchy of channels at the multi-scale endowed the HSF with a more-porous structure and considerable capacity for water infiltration. Fluorescent microscopy has been used to trace the infiltration of water into the HSF twisted from ten-ply HPFs. The micron-scaled channels among the HPFs were rapidly filled with a rhodamine/water solution upon contact with it (Figure S18). In other worlds, the water could be efficiently transported through the trunk micron-scaled channels and then infiltrated into the connected capillary nanoscale channels, that is, a faster mechanical responsiveness was achieved.

By virtue of the remarkable actuation performance, the HSF could be used to make smart windows which respond to environmental changes (Figure 4, Movies S2–S4). An HSF was fixed on the backside of the window frame. The upper section of the HSF was exposed to generate rotations (Figure S19 and 20). The rotary direction was tuned by the HSF chirality (Figure 4 b), so a left-handed HSF twisted from ten left-handed HPFs acted as the rotary shaft in the left window, while a right-handed HSF twisted from ten right-handed HPFs acted as the shaft of the right window (Figure S21). Driven by the reversible water-induced rotary actuations, the windows were opened and subsequently closed within 1.1 s upon absorption and evaporation of the water, respectively (Figure 4 c). Therefore, the smart window could be effectively operated in response to the change of weather, e.g., it was open in a sunny day and automatically closed due to the rotary actuation generated by the fiber upon raining; it would be opened again as raining stopped. (Figure S22). According to Figure 2 a, the actuation forces could be scaled up by increasing the number of HPFs to drive heavier windows. The actuation of HSF could also be triggered by the moisture, so it could be made into a smart louver in response to the change of humidity. The smart louver was gradually opened with the increasing humidity from 25 % to 80 % at room (Figure 4 d–f and Movie S3).

In summary, a general and effective strategy has been developed to synthesize actuating CNT fibers in response to water and moisture by designing hierarchically helical channels. These fibers display a combined rapid response, large contractive stroke and high rotation output. They are mechanically robust and suitable for various sensing applications, such as smart switches, robots, and biomimetic devices.

## *Experimental Section*

Preparation of hydrophilic fibers: The primary CNT fibers were modified through the oxygen microwave plasma at a pressure of 0.1 mbar and flow rate of oxygen gas of 300 sccm (Plasma System 690, PVA Tepla). The powers and times were ranged from 100 to 400 W and 15 to 45 min, respectively. The helical angles were increased by increasing the twisting speeds, e.g., 8°, 13°, 20°, 28°, 31°, and 43° at rotary speeds of 500, 1000, 1500, 2000, 2500, and 3000 revolutions per minute, respectively. The primary fiber with a helical angle of 0° was directed prepared from CNT sheet by passing it through ethanol without twisting. The primary fibers were further collected by a rotating drum with a speed of 15 cm $min^{-1}$. Multiply HPFs were bundled together with one end fixed at a rotating motor shaft and the other at a movable object. They were twisted into an HSF by rotating the motor shaft at a speed of 100 rpm with the fiber being maintained horizontal and straight. Typically, an HSF with a length of ca. 7.5 cm was obtained from multi-ply HPFs with length of 10 cm.

Characterization: The structures were characterized by scanning electron microscopy (Hitachi FE-SEM S-4800), transmission electron

microscope (JEOL JEM-2100F) and Raman spectrometer (XploRA, HORIBA JobinYvon, France). X-ray photoelectron spectroscopy measurements were performed in Axis Ultra DLD from Kratos, equipped with a monochromatic $Al_{K\alpha}$ X-ray source. Photographs and videos were recorded by a digital camera (Nikon J1). The mechanical tests of the fibers were carried out on the HY0350 Table-top Testing Instrument with a tensile speed of 1 mm $min^{-1}$. The fibers were fixed on a paper hole with a gauge length of 5 mm by silver paste. The water-induced contractive stress was traced by the same instrument. For the rotary actuation measurement, two iron paddles with weights of 21 and 99 mg were fixed at the middle of the fiber with a length of ca. 1 cm. A red label was attached at one side of the paddle to count the revolution number. Through a frame-by-frame analysis, the rotary revolution ($\theta$) was calculated by equation of $\theta = 90°\text{-}\arcsin(d/l)$, where $l$ and $d$ correspond to the length of the red paper and actual length derived from the frame photograph, respectively.

## Acknowledgements

This work was supported by MOST (2011CB932503), NSFC (21225417, 61136003), STCSM (12nm0503200, 15XD1500400), Fok Ying Tong Education Foundation, the Program for Special Appointments of Professors at Shanghai Institutions of Higher Learning, and the Program for Outstanding Young Scholars from the Organization Department of the CPC Central Committee.

**Keywords:** actuating · carbon nanotubes · fiber · hierarchical channels · water sensors

**How to cite:** *Angew. Chem. Int. Ed.* **2015**, *54*, 14880–14884
*Angew. Chem.* **2015**, *127*, 15093–15097

[1] a) E. Reyssat, L. Mahadevan, *J. R. Soc. Interface* **2009**, *6*, 951–957; b) T. D. Wheeler, A. D. Stroock, *Nature* **2008**, *455*, 208–212; c) D. Cosgrove, E. Steudle, *Planta* **1981**, *153*, 343–350; d) J. Dumais, Y. Forterre, *Annu. Rev. Fluid Mech.* **2012**, *44*, 453–478.

[2] a) P. F. Scholander, E. D. Bradstreet, E. Hemmingsen, H. Hammel, *Science* **1965**, *148*, 339–346; b) C. Dawson, J. F. Vincent, A.-M. Rocca, *Nature* **1997**, *390*, 668–668; c) R. Elbaum, L. Zaltzman, I. Burgert, P. Fratzl, *Science* **2007**, *316*, 884–886.

[3] a) P. Fratzl, F. G. Barth, *Nature* **2009**, *462*, 442–448; b) P. Fratzl, R. Elbaum, I. Burgert, *Faraday Discuss.* **2008**, *139*, 275–282; c) J. Färber, H. Lichtenegger, A. Reiterer, S. Stanzl-Tschegg, P. Fratzl, *J. Mater. Sci.* **2001**, *36*, 5087–5092.

[4] a) K. J. Niklas, *Plant biomechanics*: *an engineering approach to plant form and function*, University of Chicago press, Chicago, **1992**; b) L. J. Gibson, M. F. Ashby, B. A. Harley, *Cellular materials in nature and medicine*, Cambridge University Press, Cambridge, **2010**.

[5] J.-S. Wang, G. Wang, X.-Q. Feng, T. Kitamura, Y.-L. Kang, S.-W. Yu, Q.-H. Qin, *Sci. Rep.* **2013**, *3*, 3102.

[6] L. J. Gibson, *J. R. Soc. Interface* **2012**, *9*, 2749–2766.

[7] a) Y. Zhou, N. Sharma, P. Deshmukh, R. K. Lakhman, M. Jain, R. M. Kasi, *J. Am. Chem. Soc.* **2012**, *134*, 1630–1641; b) D. J. Broer, C. M. Bastiaansen, M. G. Debije, A. P. Schenning, *Angew. Chem. Int. Ed.* **2012**, *51*, 7102–7109; c) B. Chen, C. T. Riche, M. Lehmann, M. Gupta, *ACS Appl. Mater. Interfaces* **2012**, *4*, 6911–6916; d) J. Abel, J. Luntz, D. Brei, *Smart Mater. Struct.* **2013**, *22*, 125001; e) G. Wu, G. Li, T. Lan, Y. Hu, Q. Li, T. Zhang, W. Chen, *J. Mater. Chem. A* **2014**, *2*, 16836–16841; f) J. Ueda, T. W. Secord, H. H. Asada, *IEEE/ASME Trans. Mechatron.* **2010**, *15*, 770–782.

[8] a) V. Merk, M. Chanana, N. Gierlinger, A. M. Hirt, I. Burgert, *ACS Appl. Mater. Interfaces* **2014**, *6*, 9760–9767; b) F. Liu, M. W. Urban, *Prog. Polym. Sci.* **2010**, *35*, 3–23.

[9] a) A. A. Balandin, *Nat. Mater.* **2011**, *10*, 569–581; b) M.-F. Yu, B. S. Files, S. Arepalli, R. S. Ruoff, *Phys. Rev. Lett.* **2000**, *84*, 5552; c) P. G. Collins, P. Avouris, *Sci. Am.* **2000**, *283*, 62–69.

[10] a) K. Jiang, Q. Li, S. Fan, *Nature* **2002**, *419*, 801–801; b) P. Chen, Y. Xu, S. He, X. Sun, S. Pan, J. Deng, D. Chen, H. Peng, *Nat. Nanotechnol.* **2015**, *10*, DOI: 10.1038/NNANO.2015.198; c) X. Zhang, Q. Li, T. G. Holesinger, P. N. Arendt, J. Huang, P. D. Kirven, T. G. Clapp, R. F. DePaula, X. Liao, Y. Zhao, Y. T. Zhu, *Adv. Mater.* **2007**, *19*, 4198–4201.

[11] a) W. Guo, C. Liu, F. Zhao, X. Sun, Z. Yang, T. Chen, X. Chen, L. Qiu, X. Hu, H. Peng, *Adv. Mater.* **2012**, *24*, 5379–5384; b) M. D. Lima, N. Li, M. J. de Andrade, S. L. Fang, J. Oh, G. M. Spinks, M. E. Kozlov, C. S. Haines, D. Suh, J. Foroughi, S. J. Kim, Y. S. Chen, T. Ware, M. K. Shin, L. D. Machado, A. F. Fonseca, J. D. W. Madden, W. E. Voit, D. S. Galvao, R. H. Baughman, *Science* **2012**, *338*, 928–932; c) J. Foroughi, G. M. Spinks, G. G. Wallace, J. Oh, M. E. Kozlov, S. Fang, T. Mirfakhrai, J. D. Madden, M. K. Shin, S. J. Kim, R. H. Baughman, *Science* **2011**, *334*, 494–497; d) F. Meng, X. Zhang, R. Li, J. Zhao, X. Xuan, X. Wang, J. Zou, Q. Li, *Adv. Mater.* **2014**, *26*, 2480–2485; e) J. A. Lee, Y. T. Kim, G. M. Spinks, D. Suh, X. Lepró, M. c. D. Lima, R. H. Baughman, S. J. Kim, *Nano Lett.* **2014**, *14*, 2664–2669.

[12] L. Qiu, X. Sun, Z. Yang, W. Guo, H. Peng, *Acta Chim. Sin.* **2012**, *70*, 1523–1532.

[13] a) F. Meng, J. Zhao, Y. Ye, X. Zhang, Q. Li, *Nanoscale* **2012**, *4*, 7464–7468; b) X. Fang, Z. Yang, L. Qiu, H. Sun, S. Pan, J. Deng, Y. Luo, H. Peng, *Adv. Mater.* **2014**, *26*, 1694–1698.

[14] T. Mirfakhrai, J. D. Madden, R. H. Baughman, *Mater. Today* **2007**, *10*, 30–38.

[15] Y. Huang, J. Liang, Y. Chen, *J. Mater. Chem.* **2012**, *22*, 3671–3679.

[16] H. Cheng, Y. Hu, F. Zhao, Z. Dong, Y. Wang, N. Chen, Z. Zhang, L. Qu, *Adv. Mater.* **2014**, *26*, 2909–2913.

[17] a) A. C. Keefe, G. P. Carman, *Smart Mater. Struct.* **2000**, *9*, 665; b) Y. Fang, T. J. Pence, X. Tan, *IEEE/ASME Trans. Mechatron.* **2011**, *16*, 656–664.

[18] I. W. Hunter, J. M. Hollerbach, J. Ballantyne, *Robotics Rev.* **1991**, *2*, 299–342.

Received: July 31, 2015
Published online: October 13, 2015

  